Nano Research
DOI 10.1007/s12274-013-0294-x
Research Article
ISSN 1998-0124
CN 11-5974/O4

Coaxial Si/anodic titanium oxide/Si nanotube arrays for lithium-ion battery anode

Jiepeng Rong[1,§], Xin Fang[1,§], Mingyuan Ge[1], Haitian Chen[2], Jing Xu[1], and Chongwu Zhou[2] (✉)

Nano Res., **Just Accepted Manuscript** • DOI: 10.1007/s12274-013-0294-x
http://www.thenanoresearch.com on January 12, 2013

Just Accepted

Coaxial Si / Anodic Titanium Oxide / Si Nanotube Arrays for Lithium-ion Battery Anode

JiepengRong,[†,§]Xin Fang,[†,§]MingyuanGe,[†] Haitian Chen,[‡] Jing Xu,[†] and Chongwu Zhou[‡,*]

[†]Mork Family Department of Chemical Engineering and Materials Science and [‡] Ming Hsieh Department of Electrical Engineering, University of Southern California, Los Angeles, California 90089, United States

§These authors contributed equally to this paper.

Address correspondence to chongwuz@usc.edu

Page Numbers.

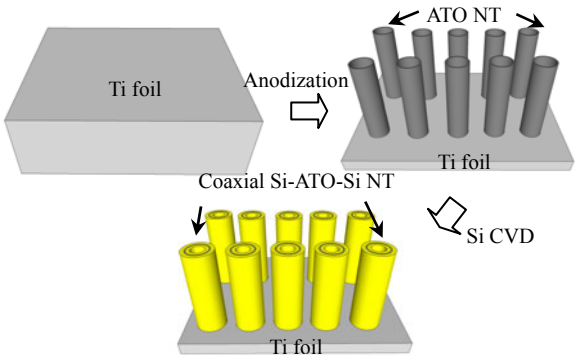

Here, we report a coaxial silicon / anodic titanium oxide / silicon (Si-ATO-Si) nanotube array structure grown on titanium substrate demonstrating excellent electrochemical cyclability. This coaxial structure shows a capacity above 1500 mAh/g after 100 cycles, with less than 0.05% decay per cycle.

Provide the authors' website if possible.

Chongwu Zhou*, nanolab.usc.edu

Nano Res
DOI (automatically inserted by the publisher)
Research Article

Coaxial Si / Anodic Titanium Oxide / Si Nanotube Arrays for Lithium-ion Battery Anode

Jiepeng Rong,[1,§] Xin Fang,[1,§] Mingyuan Ge,[1] Haitian Chen,[2] Jing Xu,[1] and Chongwu Zhou[2] (✉)

[1] Mork Family Department of Chemical Engineering and Materials Science, University of Southern California, Los Angeles, California 90089, United States
[2] Ming Hsieh Department of Electrical Engineering, University of Southern California, Los Angeles, California 90089, United States
[§] These authors contributed equally to this paper.

Received: day month year / Revised: day month year / Accepted: day month year (automatically inserted by the publisher)

ABSTRACT

Silicon (Si) has the highest known theoretical specific capacity (3590 mAh/g for $Li_{15}Si_4$, and 4200 mAh/g for $Li_{22}Si_4$) as lithium-ion battery anode, and has attracted extensive interest in the past few years. However, its application is limited by poor cyclability and early capacity fading due to significant volume change during lithiation and delithiation process. In this work, we report a coaxial silicon / anodic titanium oxide / silicon (Si-ATO-Si) nanotube array structure grown on titanium substrate demonstrating excellent electrochemical cyclability. The ATO nanotube scaffold used for Si deposition has many desired features, such as rough surface for enhanced Si adhesion, and direct contact with the Ti substrate working as current collector. More importantly, our ATO scaffold provides a rather unique advantage that Si can be loaded on both the inner and outer surfaces, and an inner pore can be maintained to provide room for Si volume expansion. This coaxial structure shows a capacity above 1500 mAh/g after 100 cycles, with less than 0.05% decay per cycle. This improved performance could be attributed to the low stress induced to Si layer upon lithiation/delithiation compared with some other Si-based nanostructures recently reported, which is further proved by simulation.

KEYWORDS

Lithium ion battery; anodic titanium oxide; silicon anode

1. Introduction

Increasing efforts have been devoted to the development of lithium-ion batteries with higher energy density, higher charging and discharging rate, and longer cycle life to meet the requirement of ever growing portable electronic and next-generation electrical vehicles industry [1-13]. Silicon has drawn particular attention as anode material for lithium-ion batteries primarily because it has the highest known theoretical capacity (3590 mAh/g for $Li_{15}Si_4$, and 4200 mAh/g for $Li_{22}Si_4$), which is nine times higher than that of commercial graphite anodes and other oxide and nitride materials [14]. However, its application is restricted by severe capacity fading caused by pulverization, which is due to large volume expansion and contraction during lithiation and delithiation process ($Si + xLi^+ + xe^- \rightarrow Li_xSi$ ($0 \le x \le 4.4$)).

Thus far, it has been evidenced that nanostructured Si could be utilized to obtain improved electrochemical performance over bulk Si and is considered as promising candidates for high performance lithium-ion battery anodes, such as Si nanowires (NWs) [15-17], carbon-Si core-shell NWs [18], carbon-Si nanocomposites [19,20], TiSi2/Si nanonets [21], three-dimensional porous Si [22,23], and sealed Si nanotubes [24]. These studies indicate that the key feature for electrode design is providing enough free space around Si so that large volume expansion could be accommodated. In addition, Si nanostructures grown directly on metallic current collector would enhance both power density and energy density of lithium-ion battery by minimizing internal resistance and the usage of non-active materials, such as carbon black and binder.

Here we report a coaxial silicon / anodic titanium oxide / silicon (Si-ATO-Si) nanotube array electrode in which anodic titanium oxide (ATO) nanotubes were rooted on titanium (Ti) current collector as the inert scaffold in the voltage window 0.01V-1V vs Li/Li^+, and the outer and inner Si shell worked as active material to store Li^+ (as shown in Figure 1g). This novel coaxial design incorporated all the key features of designing high performance lithium-ion battery anode. ATO scaffold provide a rough surface for improved Si adhesion, and direct contact with the Ti substrate working as current collector. More importantly, Si layers were coated on both outer and inner surface of ATO nanotube array scaffold, leaving abundant space between nanotubes as well as inside each tube, which allowed for better accommodation of volume expansion outward and inward. We first used theoretical modeling to confirm our assumption that coaxial Si-ATO-Si nanotube has superior mechanical stability compared with some other Si-based nanostructures recently reported. Experimentally fabricating coaxial Si-ATO-Si nanotube array electrodes and measuring electrochemical performance as lithium-ion battery anode further validated the feasibility of our proposal. We have achieved high first discharge (lithiation) capacity of 2824 mAh/g at the current density of 140 mA/g and long-cycling test after that achieved stable cycling performance with capacity over 1500 mAh/g at 1400 mA/g current rate, which means less than 5% capacity degradation for 100 cycles. Excellent rate capability was also demonstrated.

2. Results and Discussion

2.1. Numerical Simulation Results

Finite element modeling has been recently explored to numerically simulate stress evolution in electrode materials to help us better understand the process of high-stress buildup [25]. The high-stress buildup may eventually lead to mechanical fracture and isolation of electrode material from the metallic current collector, which was regarded as the key point to solve capacity fading problem associated with many electrode materials, such as Si and $LiMn_2O_4$. Here, we adapted a finite element model developed by Lu [25] to calculate the stress distribution caused by volume change due to Li^+ intercalation. By comparing the maximum stress existing in coaxial Si-ATO-Si nanotube array structure we proposed here with other two types of high performance Si-based nanocomposites recently reported [26-28], we found the coaxial Si-ATO-Si nanotube array structure we proposed in this paper

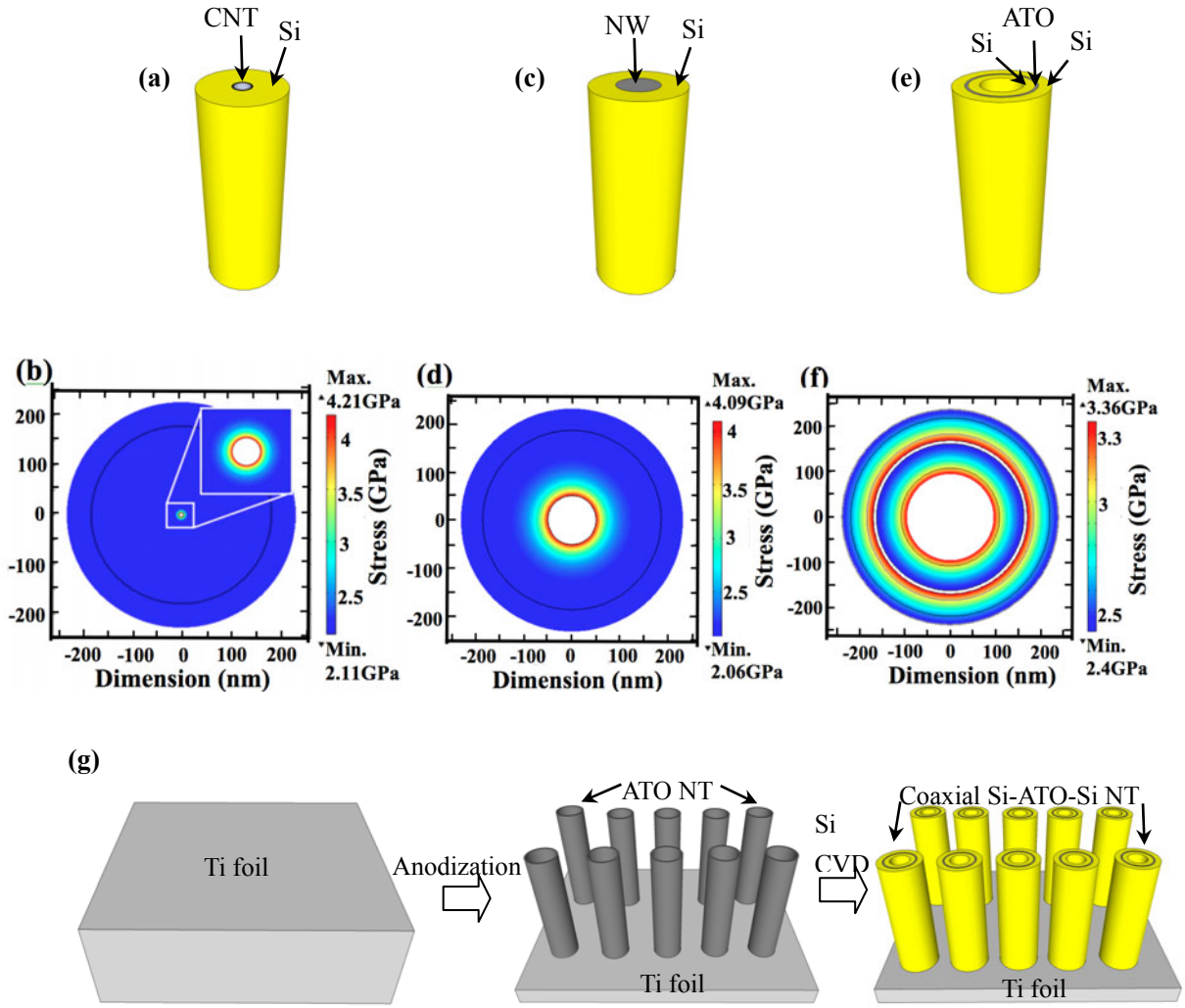

Figure 1. (a-f) Schematic diagram (a,c,e) and finite element modeling (b,d,f) of CNT-Si core-shell structure (a,b), NW-Si core-shell structure (c,d), and coaxial Si-ATO-Si nanotube structure (e,f). (g) Schematic of fabrication process of coaxial Si-ATO-Si nanotube structure.

have the lowest maximum hydrostatic stress indicating it has lowest risk of mechanical fracture and highest stability during charge/discharge cycling. The three nanocomposites we studied are (1) carbon nanotube (CNT)-Si core-shell structure [26], with 10nm CNT diameter (Figure 1a,b), (2) nanowire (NW)-Si core-shell structure, with 100nm NW diameter (Figure 1c,d), where the inner NW can be TiC NW [27] or copper NW [28], and (3) coaxial Si-ATO-Si nanotube structure, with 300nm and 340nm as ATO nanotube inner diameter and outer diameter (Figure 1e,f). In our model, the loading of Si was the same on unit length of CNT, NW and ATO nanotube, which was calculated to be 174 nm and 136 nm thick Si layer on CNT and NW respectively, and 50 nm on both inner and outer surface of ATO nanotube. Considering the uniformity in the longitude direction of all three nanocomposites, the calculation was carried out on two-dimensional cross-section. ATO nanotubes do not participate in lithiation/delithiationafter the first cycle between 0.01 V-1 V and therefore experience no volume change. Thus, in the numerical simulation, ATO nanotubes are fixed in

dimension.

The elastic field was taken into consideration when solving the diffusion problem to obtain the concentration and stress profile. The diffusion flux **J** is given by,

$$\mathbf{J}=-D(\nabla c-(\Omega c/RT)\nabla\sigma_h) \quad (1)$$

where c is concentration of lithium ions, D is diffusion coefficient, R is the gas constant, T is the absolute temperature, σ_h is the hydrostatic stress, and Ω is the partial molar volume. The two terms on the right side of the equation above take care of the effect of Li^+ concentration gradient and stress gradient due to Li^+ insertion.

Applying mass conservation equation, $\partial c/\partial t+\nabla\bullet\mathbf{J}=0$, we could get hydrostatic stress σ_h satisfying,

$$\partial c/\partial t-\nabla\bullet(D(\nabla c-(\Omega c/RT)\nabla\sigma_h))=0 \quad (2)$$

The hydrostatic stress could be calculated and mapped using FEMLAB (COMSOL Multiphysics) by applying a constant current boundary condition

$$\mathbf{J}\bullet\mathbf{n}=i_n/F \quad (3)$$

where **n** is the normal vector of the surface, i_n is the current density, and F is Faraday's constant.

The hydrostatic stress profiles of three structures in Figure 1a, c and e were plotted in Figure 1b, d and f, respectively. The maximum hydrostatic stress existed in (1) CNT-Si core-shell structure (Figure 1b), (2) NW-Si core-shell structure (Figure 1d), and (3) coaxial Si-ATO-Si nanotube structure (Figure 1f) are 4.2, 4.1 and 3.4 GPa, respectively. The corresponding composition is $Li_{15}Si_4$ for all structures. The positions of the maximum stress were located at the most inner layer of Si shell for all three cases. The structures we proposed in this paper had lowest maximum hydrostatic stress, indicating it had lowest risk of mechanical fracture and highest stability during charge/discharge cycling. This may result from the difference in Si-layer thickness. Coaxial Si-ATO-Si nanotube structure had the thinnest Si-layer thickness of 50 nm on both inner and outer side of ATO tubes, as well as the smallest maximum stress of 3.4 GPa. In comparison, CNT-Si core-shell structure had the thickest Si-layer thickness of 174 nm and the largest maximum stress of 4.2 GPa. We stress that our ATO scaffolds provide a rather unique advantage that silicon can be loaded both on inner and outer surface, and an inner pore can still be maintained to provide space for silicon volume expansion. Those features cannot be obtained with the CNT or NW scaffold structures.

2.2. Electrode Fabrication and Characterization

Coaxial Si-ATO-Si nanotube array electrode was experimentally fabricated by employing a template approach using ATO nanotubes, as shown by the schematic in Figure 1g. ATO scaffold was first prepared by anodization of Ti foil [29], and it provided both mechanical support as well as charge transport path for the active amorphous Si layer on both inner and outer surface. In addition, ATO nanotube does not react with lithium in the voltage window 0.01V-1V *vs* Li/Li^+, which has been confirmed by our cyclic voltammetry (CV) measurements (Figure 3a). We successfully got ATO nanotubes with 100 nm to 300 nm in diameter and 1 μm to 10 μm in length by utilizing different reaction time and voltage. Then, an amorphous Si layer, functioning as the Li storage media, was conformally coated on the surface of ATO nanotube scaffold by chemical vapor deposition (CVD). In this way, the weight ratio of the Si

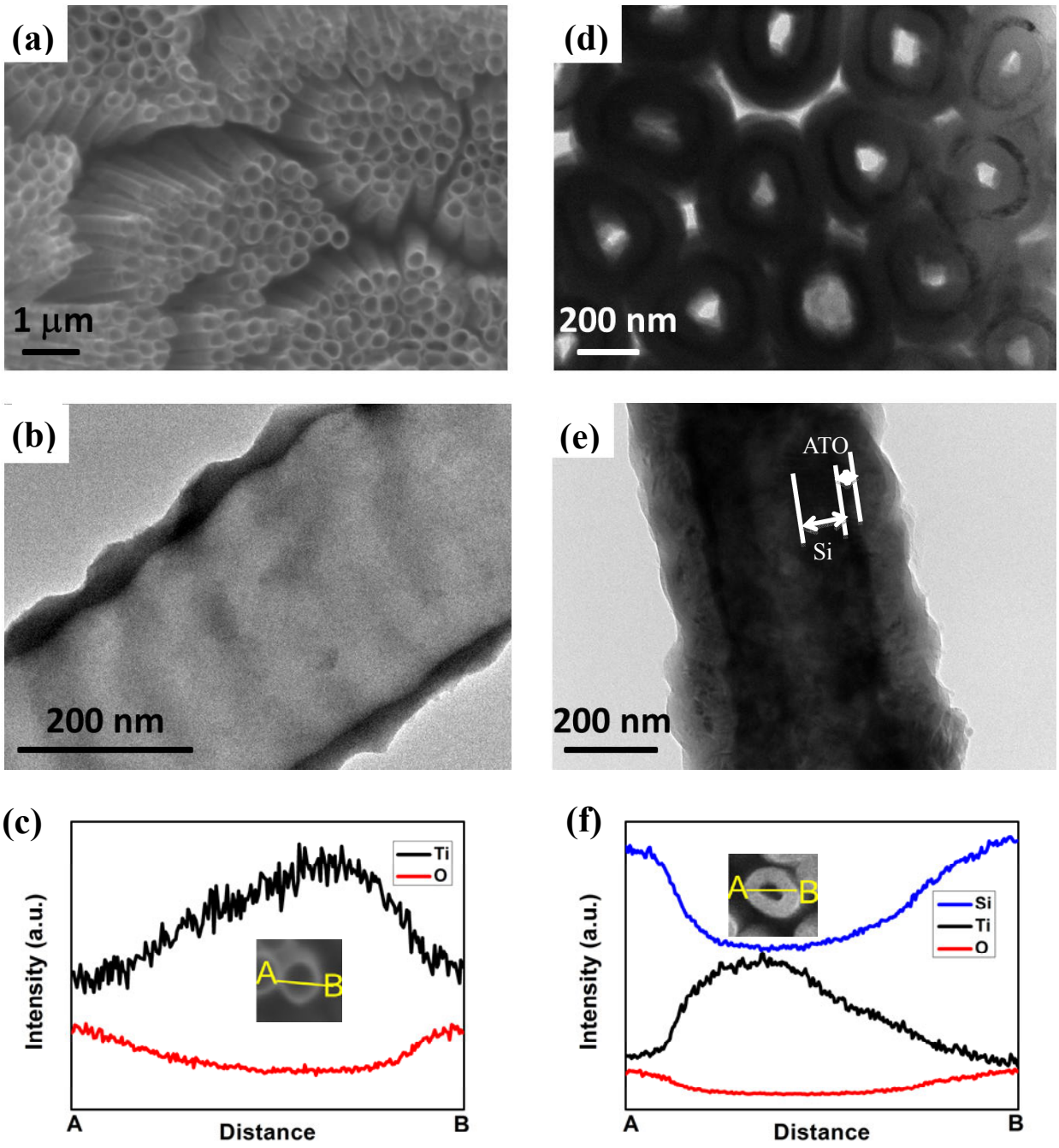

Figure 2. Characterization of ATO and coaxial Si-ATO-Si nanotubes. (a) SEM of as-prepared ATO nanotubes on a Ti substrate. (b) TEM image of an as-prepared ATO nanotube. (c) Line scan profile over an ATO nanotube (from point A to B in Figure 2c inset). (d) TEM image of the cross-section view of a coaxial Si-ATO-Si nanotube. (e) TEM image of the side view of a coaxial Si-ATO-Si nanotube. (f) Line scan profile over an coaxial Si-ATO-Si nanotube (from point A to B in Figure 2f inset).

layers to the ATO scaffold could be tuned by varying the thickness of Si coating, which could be easily controlled by CVD time. Si layer needs to be thick enough to provide reasonable loading and thinner than the fracture threshold to avoid losing structural integrity during

lithiation-delithiation cycling. Different Si layer thicknesses ranging from 20 nm to 80 nm and different ATO nanotube lengths were tested, and no obvious difference in terms of electrochemical performance was observed.

The morphology and composition of as-synthesized ATO nanotube array was first characterized by scanning electron microscopy (SEM). Figure 2a shows that vertically aligned ATO nanotube array with uniform diameter could be obtained. The morphology of ATO nanotubes was further characterized by transmission electron microscopy (TEM), as shown in Figure 2b. The ATO nanotubes have an inner radius (R_{in}) of 150 nm and an outer radius (R_{out}) of 170 nm. The rough external and internal surface of ATO nanotubes, intrinsically resulted from the anodization process, would be beneficial to enhance the adherence of Si, which was proven to be a key factor to govern the electrochemical performance of lithium-ion batteries [19,30-34].The element distribution in ATO nanotubes was analyzed by energy dispersive X-ray (EDX) spectroscopy line scan over the cross-section of one nanotube (Figure 2c). The opposite trend of signal intensity between oxygen (O) and Ti over scanning distance is because O signal is solely from ATO, while Ti is from both ATO and Ti substrate beneath, which could explain why Ti exhibits higher signal intensity over the void space in the center. Coaxial Si-ATO-Si nanotubes were fabricated by Si deposition on ATO nanotubes by CVD. Coaxial Si-ATO-Si nanotube fragments were generated by performing sonication on coaxial Si-ATO-Si nanotube array and characterized by TEM, as shown in Figure 2d. Both cross-section view (Figure 2d) and side view (Figure 2e) revealed a coaxial Si-ATO-Si structure with 50 nm uniform conformal Si coating on both inner and outer surface of ATO nanotubes. Si distribution was investigated by EDX (Figure 2f), confirming that Si symmetrically distributed on both inner and outer surface of ATO nanotubes. After 50 nm Si coated on ATO nanotubes, few-nanometers thick Si at the surface will be oxidized to SiO_x when exposed to air. Oxygen signals in EDX results could be from both the thin layer of SiO_x and ATO nanotube inside.

2.3. Electrochemical Measurements

After fabrication of coaxial Si-ATO-Si nanotube array on Ti substrate, we evaluated its electrochemical performance. Figure 3a shows typical cyclic voltammetry (CV) curves of the ATO nanotube array scaffold before and after Si deposition over the voltage window of 0.01V-1V *vs* Li/Li^+ at a scan rate of 0.1 mV/s. ATO nanotubes with no Si coating exhibited electrochemical double-layer capacitor behavior with no peak related to reaction with lithium, which confirmed the inactive nature of ATO as a scaffold. Although titanium oxide is a widely studied anode material reacting with lithium as $TiO_2 + xLi^+ + xe^- \leftrightarrow Li_xTiO_2$ at 1.7 V *vs* Li/Li^+ [35], we limited the voltage window between 0.01V-1V vs Li/Li^+ for both CV and galvanostatic charge/discharge measurements, so TiO_2 did not participate in lithiation/delithiation reaction with lithium and hence ATO just functioned as inert scaffold in this study. After Si deposition, the shape of CV curve changed dramatically, and signature peaks of Si-Li alloy/dealloy reactions were observed. The peak at 0.19 V in the cathodic branch (lithiation) corresponds to the conversion of amorphous Si to Li_xSi. In the anodic branch (delithiation), the two peaks at 0.35 V and 0.52 V are attributed to the delithiation of Li_xSi back to amorphous Si [36].

Two-electrode 2032 type coin cells were assembled with coaxial Si-ATO-Si nanotube array

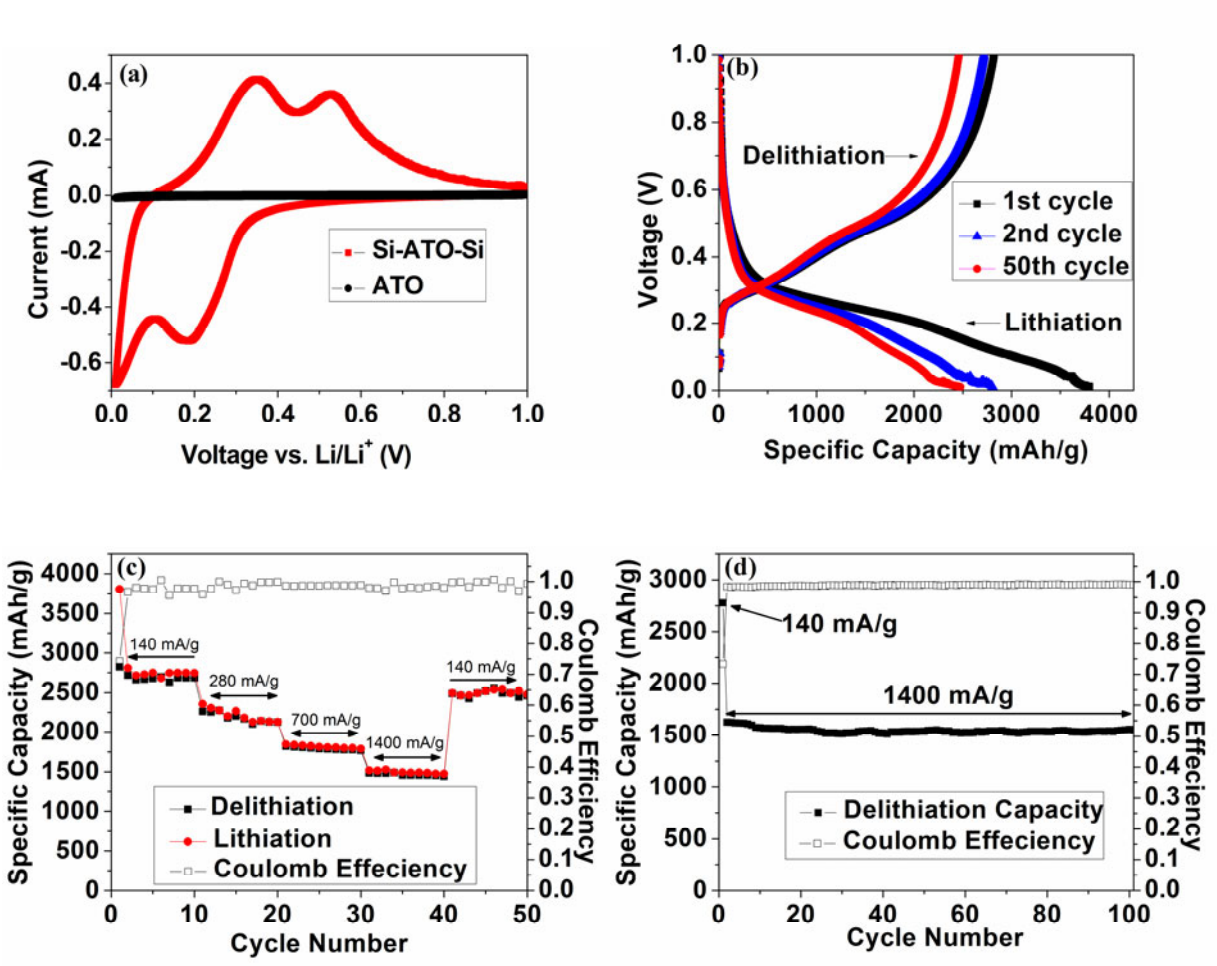

Figure 3. Electrochemical performance of a coaxial Si-ATO-Si nanotube anode. (a) Typical cyclic voltammetry curve comparison of the ATO scaffold and coaxial Si-ATO-Si nanotube, showing the inert nature of ATO with Li^+ between 0.01V-1V *v.s.* Li/Li^+. (b) Galvanostatic charge-discharge voltage profile between 0.01V-1V *vs.* Li/Li^+ for the 1^{st} , 2^{nd} , and 50^{th} cycle at 140 mA/g. (c) Charge-discharge specific capacity and Coulombiceffeciency*v.s.* cycle number for 50 cycles at different rates ranging from 140 mA/g to 1400 mA/g. Only the weight of Si is considered for specific capacity calculation. (d) Discharge specific capacity and Coulombiceffeciency*v.s.* cycle number at 1400 mAh/g with voltage window between 0.01V-1V v.s. Li/Li^+, in which condition it takes around 1 hour to charge or discharge the battery.

grown on Ti current collector as working electrode and lithium metal as the counter electrode to investigate its electrochemical performance. No binder or carbon black additives were employed. Teklon® polymer separator was used in our coin cells. 1.0 M $LiPF_6$ in 1:1 w/w ethylene carbonate/diethyl carbonate was used as electrolyte. Figure 3b shows the voltage profile for the 1^{st}, 2^{nd}, and 50^{th} cycle of galvanostatic charge/discharge measurement at the same current rate of 140 mAh/g. For the first discharge (lithiation) and charge (delithiation), specific capacity reached 3803 mAh/g and 2802 mAh/g respectively, taking only Si mass into calculation. The Coulombic efficiency in the first cycle was 73.7% and approached above 95% at all charge/discharge rates after the first cycle. The limited Coulombic efficiency in the first cycle and the improved performance thereafter could be resulted from the formation of solid electrolyte

interphase (SEI) on the electrode surface, which would consume Li^+ in an irreversible manner. In addition, the silicon oxide (SiO_x) formed on Si surface during its exposure to air could also contribute to the restricted Coulombic efficiency in the first cycle. The reaction between SiO_x and lithium is partially reversible, and the reversibility depends on the x value following the formula, $SiO_x + 2x\ Li^+ \leftrightarrow Si + x\ Li_2O$ [37,38]. Both processes mentioned above mainly happened in the first cycle and were then suppressed or slowed down, thus resulting in the limited Coulombic efficiency in the first cycle and significant improvement afterwards.

As shown in Figure 3c, the coaxial Si-ATO-Si nanotube array electrode exhibited stable cycling performance at different current rates of 140, 280, 700, and 1400 mA/g. The discharge capacities at each current rate were 2717, 2260, 1823, and 1480 mAh/g, respectively. The discharge capacity at 1400mA/g, at which rate it took around 1 hour to fully discharge/charge the battery, was higher than the theoretical capacity of graphite electrode by a factor of four. The long cycle performance of coaxial Si-ATO-Si nanotube array electrode was also explored by continuously charge and discharge at 1400 mA/g for 100 cycles after the first cycle (Figure 3d). The discharge capacity for the second and the 101st cycle were 1624 and 1548 mAh/g respectively, corresponding to 4.7% degradation for 100 cycles or less than 0.05% decay per cycle, indicating a superior cycling stability of the electrode. The retaining capacity of 1548 mAh/g after 100 charge/discharge cycles was still more than 4 times higher than the theoretical capacity of graphite. Besides the high gravimetric specific capacity achieved, volumetric specific capacity is estimated around 2800 mAh/cm^3, around 3.5 times of that of graphite (800 mAh/cm^3). (Refer to supporting information for calculation) The electrode also demonstrated favorable Coulombic efficiency, which rapidly recovered to over 98% after the first cycle, and further increased to more than 99% after 10 cycles.

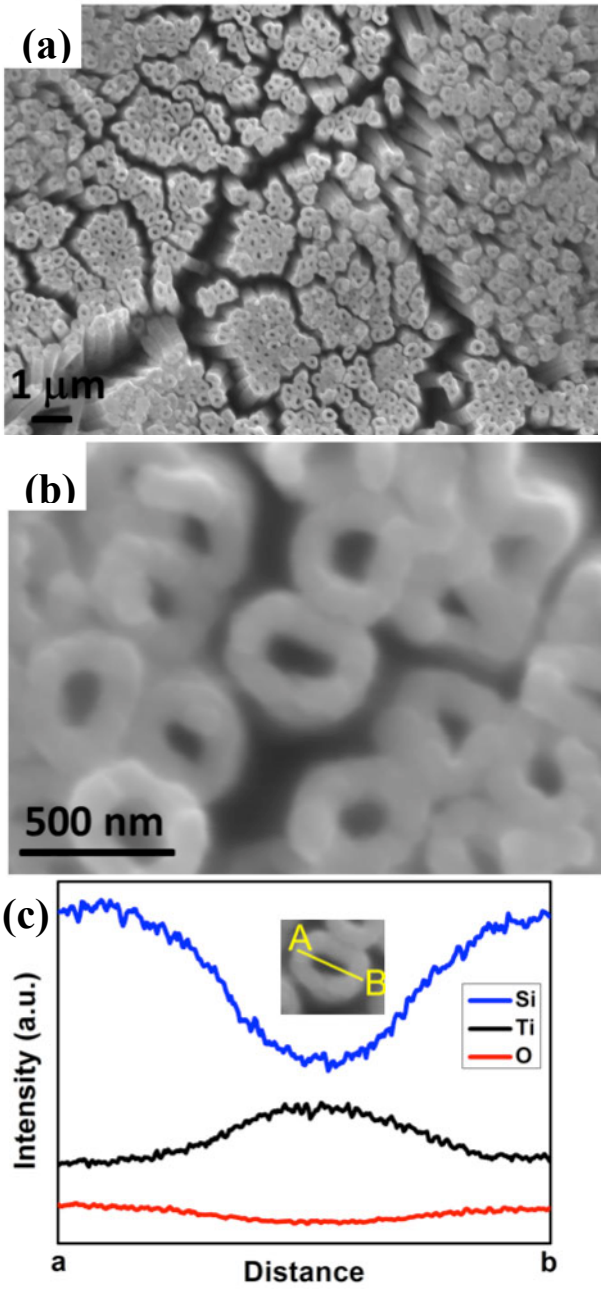

Figure 4. (a, b) SEM image of coaxial Si-ATO-Si nanotubes after 10 charge-discharge cycles and rinsed in acetonitrile and 1M HCl consecutively to remove residue electrolyte and SEI. (c) EDX line scan profile of Si (blue), Ti (black) and O (red) over one coaxial Si-ATO-Si nanotube (from point A to B in Figure 4c inset).

The excellent electrochemical performance of the coaxial Si-ATO-Si nanotube array electrode could be attributed to: (1) the ATO nanotube array provided an excellent inactive, mechanically strong scaffold and survived charge/discharge cycling intact. (2) The ATO nanotube scaffold provided direct contact with the Ti substrate working as current collector. This design could enhance both power density and energy density of lithium-ion battery by minimizing internal resistance and the usage of non-active materials. (3) The rough surface and special geometry of ATO nanotubes not only provided an ideal interface for enhanced adhesion between Si and ATO, but also behaved as a superior host of Si with lower stress associated with lithiation. (4) Si could be loaded on both the inner and outer surface of ATO scaffolds, and an inner pore can be maintained to provide room for Si volume expansion. In addition to the justification by simulation and battery performance above, these effects could be further confirmed as following. Batteries with coaxial Si-ATO-Si nanotube array electrode were disassembled after 10 charge/discharge cycles, and rinsed with acetonitrile and 1 M HCl consecutively to remove residue electrolyte and SEI. The morphology and composition were characterized with SEM and EDX. As we expected, coaxial Si-ATO-Si nanotube array electrode also showed limited change in terms of morphology and composition after cycling, which agreed with the stable cycling performance we observed. SEM images (Figure 4 a, b) and EDX line scan profile of Si (blue), Ti (black), and O (red) (Figure 4c) confirmed the coaxial Si-ATO-Si nanotube array electrode survived charge/discharge cycling intact.

3. Conclusion

In summary, we successfully fabricated coaxial Si-ATO-Si nanotube array structures and applied this novel structure to lithium-ion battery anode. The coaxial Si-ATO-Si nanotube array demonstrated high specific capacity and excellent cycling performance. After 100 cycles, the capacity still remained above 1500mAh/g and the capacity decay was less than 0.05% per cycle. This excellent cycling stability was due to the unique coaxial structure in which ATO provided a strong inert scaffold, a rough surface for Si adhesion, and the low stress upon lithiation of the Si layer by maintaining an inner pore, which was also proven by simulation. This novel structure thus can be a promising candidate for anode material to improve lithium-ion battery performance.

Experimental Methods

ATO nanotube array synthesis

The ATO nanotube array was directly formed on a Ti substrate by potentiostaticanodization at 70 V *vs* a carbon counter elecreode in diethylene glycol electrolyte (DEG) containing 1% HF. The anodization was continously carried out for 19 hours at room temperature. After anodization, the ATO nanotube array on top of Ti substrate was rinsed with ethanol and naturally dried in air.

Coaxial Si-ATO-Si nanotube synthesis

An amorphous Si layer, functioning as the Li storage media, was deposited on ATO nanotube scaffold by chemical vapor deposition (CVD) of silane (2% SiH_4 balanced in Ar) at 530 ^oC for 10 min in a quartz tube furnace (1 inch diameter). The total chamber pressure was 100 Torr. Thickness of Si coating could be easily controlled by reaction time.

Acknowledgements

We acknowledge the University of Southern California for financial support.

Electronic Supplementary Material:
Supplementary material (analysis of first lithiation, parameters used in simulation) is available in the online version of this article at http://dx.doi.org/10.1007/s12274-***-****-*

References

[1]. Scrosati, B. Battery Technology—Challenge of Portable Power. *Nature* 1995, 373, 557-558.

[2]. Tarascon, J. M.; Armand, M. Issues and Challenges facing Rechargeable Lithium Batteries. *Nature* 2001, 414, 359-367.

[3]. Armand, M.; Tarascon, J. M. Building Better Batteries. *Nature* 2008, 451, 652-657.

[4]. Rolison, D. R.; Nazar, L. F. Electrochemical Energy Storage to Power the 21st Century. *MRS Bull.* 2011, 36, 486-493.

[5]. Goodenough, J. B.; Kim, Y. Challenges for Rechargeable Li Batteries. *Chem. Mater.* 2010, 22, 587-603.

[6]. Liu J.; Cao, G.; Yang, Z.; Wang, D.; Dubois, D; Zhou, X.; Graff, G. L.; Pederson, L. R.; Zhang, J. G. Oriented Nanostructures for Energy Conversion and Storage. ChemSusChem 2008, 1, 676-697.

[7]. Oumellal, Y.; Rougier, A.; Nazri, G. A.; Tarascon, J. M.; Aymard, L. Metal Hydrides for Lithium-Ion Batteries. *Nat. Mater.* 2008, 7, 916-921.

[8]. Bruce, P. G.; Scrosati, B.; Tarascon, J. M. Nanomaterials for Rechargeable Lithium Batteries. *Angew. Chem., Int. Ed.* 2008, 47, 2930-2946.

[9]. Sun, Y. K.; Myung, S. T.; Park, B. C.; Prakash, J.; Belharouak, I.; Amine, K. High-Energy Cathode Material for Long-life and Safe Lithium Batteries. *Nat. Mater.* 2009, 8, 320-324.

[10]. Huang, J. Y.; Zhong, L.; Wang, C. M.; Sullivan, J. P.; Xu, W.; Zhang, L. Q.; Mao, S. X.; Hudak, N. S.; Liu, X. H.; Subramanian, A.; et al. In Situ Observation of the Electrochemical Lithiation of a Single SnO_2 Nanowire Electrode. *Science* 2010, 330, 1515-1520.

[11]. Ji, X.; Evers, S.; Black, R.; Nazar, L. F. Stabilizing Lithium-Sulphur Cathodes Using Polysulphide Reservoirs. *Nat. Commun.* 2011, 2, 325.

[12]. Zhang, H.; Yu, X.; Braun, P. V. Three-Dimensional Bicontinuous Ultrafast-Charge and Discharge Bulk Battery Electrodes. *Nat. Nanotechnol.* 2011, 6, 277-281.

[13]. Malik, R.; Zhou, F; Ceder, G. Kinetics of Non-Equilibrium Lithium Incorporation in $LiFePO_4$. *Nat. Mater.* 2011, 10, 587-590.

[14]. Boukamp, B. A.; Lesh, G. C.; Huggins, R. A. All-Solid Lithium Electrodes with Mixed-Conductor Matrix. *J. Electrochem. Soc.* 1981, 128, 725-729.

[15]. Chan, C. K.; Peng, H. L.; Liu, G.; Mcllwrath, K.; Zhang, X. F.; Huggins, R. A.; Cui, Y. High-Performance Lithium Battery Anodes Using Silicon Nanowires. *Nat. Nanotechnol.* 2008, 3, 31-35.

[16]. Cui, L. F.; Ruffo, R.; Chan, C. K.; Peng, H. L.; Cui, Y.; Crystalline-Amorphous Core-Shell Silicon Nanowire for High Capacity and High Current Battery Electrodes. *Nano Lett.* 2009, 9, 491-495.

[17]. Chen, H. T.; Xu, J.; Chen, P. C.; Fang, X.; Qiu, J.; Fu, Y.; Zhou, C. W. Bulk Synthesis of Crystalline and Crystalline Core/Amorphous Shell Silicon Nanowires and Their Application for Energy Storage. *ACS Nano* 2011, 5, 8383-8390.

[18]. Cui, L. F.; Yang. Y.; Hsu, C. M.; Cui, Y. Carbon-Silicon Core-Shell Nanowires as High Capacity Electrodes for Lithium Ion Batteries. *Nano Lett.* 2009, 9, 3370-3374.

[19]. Magasinski, A.; Dixon, P.; Hertzberg, B.; Kvit, A.; Ayala, J.; Yushin, G. High-Performance Lithium-Ion Anode Using a Hierarchical Bottom-Up Approach. *Nat. Mater.* 2010, 9, 353-358.

[20]. Rong, J. P.; Masarapu, C.; Ni, J.; Zhang, Z. J.; Wei, B. Q. Tandem Structure of Porous Silicon Film on

Single-Walled Carbon Nanotube Macrofilms for Lithium-Ion Battery Applications. *ACS Nano* 2010, 4, 4683-4690.

[21]. Zhou, S.; Liu, X.; Wang, D. Si/TiS_2Heteronanostructures as High-Capacity Anodes Materials for Li Ion Batteries. *Nano Lett.* 2010, 10, 860-863.

[22]. Kim, H.; Han, B.; Choo, J.; Cho, J. Three-Dimensional Porous Silicon Particles for Use in High-Performance Lithium Secondary Batteries. *Angew. Chem., Int. Ed.* 2008, 47, 10151–10154.

[23]. Yao, Y.; McDowell, M. T.; Ryu, I.; Wu, H.; Liu, N.; Hu, L.; Nix, W. D.; Cui. Y. Interconnected Silicon Hollow Nanospheres for Lithium-Ion Battery Anodes with Long Cycle Life. *Nano Lett.* 2011, 11, 2949-2954.

[24]. Song, T.; Xia, J. L.; Lee, J. H.; Lee, D. H.; Kwon, M. S.; Choi, J. M.; Wu, J.; Doo, S. K.; Chang, H.; Il Park, W.; Zang, D. S.; Kim, H.; Huang, Y. G.; Hwang, K. C.; Rogers, J. A.; Paik, U. Arrays of Sealed Silicon Nanotubes As Anodes for Lithium Ion Batteries. *Nano Lett.* 2010, 10, 1710–1716.

[25]. Park, J.; Lu, W.; Sastry, A. M. Numerical Simulation of Stress Evolution in Lithium Manganese Oxide Particles due to Coupled Phase Transition and Intercalation. *J. Electrochem. Soc.* 2011, 158, A201-206.

[26]. Evanoff, K.; Khan, J.; Balandin, A. A.; Magasinski, A.; Ready, W. J.; Fuller, T. F.; Yushin, G. Towards Ultrathick Battery Electrodes: Aligned Carbon Nanotube – Enabled Architecture. *Adv. Mater.* 2012, 24, 533-537.

[27]. Yao, Y.; Huo, K. F.; Hu, L. B.; Liu, N.; Cha, J. J.; McDowell, M. T.; Chu, P. K.; Cui, Y. Highly Conductive, Mechanically Robust, and Electrochemically Inactive TiC/C NanofiberScaffold for High-Performance Silicon Anode Batteries. *ACS Nano* 2011, 5, 8346-8351.

[28]. Cao, F. F.; Deng, J. W.; Xin, S.; Ji, H. X.; Schmidt, O. G.; Wan, L. J.; Guo, Y. G. Cu-Si Nanocable Arrays as High-Rate Anode Materials for Lithium-Ion Batteries. *Adv. Mater.* 2011, 23, 4415-4420.

[29]. Yoriya, S.; Grimes, C. A. Self-Assembled TiO2 Nanotube Arrays by Anodizationi of Titanium in Diethylene Glycol: Approach to Extended Pore Widening. *Langmuir* 2010, 26(1), 417-420.

[30]. Beaulieu, L. Y.; Eberman, K. W.; Turner, R. L.; Krause, L. J.; Dahn, J. R. Colossal Reversible Volume Changes in Lithium Alloys. *Electrochem. Solid-State Lett.* 2001, 4, A137-A140.

[31]. Park, M. S.; Wang, G. X.; Liu, H. K.; Dou, S. X. Pulsed Laser Deposition for Lithium Ion Micro-batteries. *Electrochim. Acta*2006, 51, 5246-5249.

[32]. Moon, T.; Kim, C.; Park, B. Electrochemical Performance of Amorphous-Silicon Thin Film for Lithium Rechargeable Batteries. *J. Power Sources* 2006, 155, 391-394.

[33]. Yin, J. T.; Wada, M.; Yamamoto, K.; Kitano, Y.; Tanase, S.; Sakai, T. Micrometer-Scale Amorphous Si Thin-Film Electrodes Fabricated by Electron-Beam Deposition for Li-Ion Batteries. *J. Electrochem. Soc.* 2006, 153, A472-477.

[34]. Kim, Y. L.; Sun, Y. K.; Lee, S. M. Enhanced Electrochemical Performance of Silicon-Based Anode Material by Using Current Collector with Modified Surface Morphology. *Electrochim. Acta*2008, 53, 4500-4504.

[35]. Yang, Z.; Choi, D.; Kerisit, S.; Rosso, K.M.; Wang, D.; Zhang, J.; Graff, J.; Liu, J. Nanostructures and Lithium Electrochemical Reactivity of Lithium Titanites and Titanium Oxides: A Review. *J. Power Sources* 2009, 192, 588-598.

[36]. Li, J.; Dahn, J. R. An in-situ X-ray diffraction study of the reaction of Li with crystalline Si.*J. Electrochem. Soc.* 2007, 154, A156-A161.

[37]. Chen, X.; Gerasopoulos, K.; Guo, J.; Brown, A.; Wang, C.; Ghodssi, R.; Culver, J. N. Virus-Enabled Silicon Anode for Lithium-Ion Batteries. *ACS Nano* 2010, 4, 5366-5372.

[38]. Cao, F.-F.; Deng, J.-W.; Xin, S.; Ji, H.-X.; Schmidt, O. G.; Wan, L.-J.; Guo, Y.-G. Cu-Si Nanocable Arrays as High-Rate Anode Materials for Lithium-Ion Batteries. *Adv. Mater.* 2011, 23, 4415-4420.

Electronic Supplementary Material

Coaxial Si / Anodic Titanium Oxide / Si Nanotube Arrays for Lithium-ion Battery Anode

Jiepeng Rong,[1,§] Xin Fang,[1,§] Mingyuan Ge,[1] Haitian Chen,[2] Jing Xu,[1] and Chongwu Zhou[2](✉)

[1]Mork Family Department of Chemical Engineering and Materials Science, University of Southern California, Los Angeles, California 90089, United States
[2]Ming Hsieh Department of Electrical Engineering, University of Southern California, Los Angeles, California 90089, United States
[§]These authors contributed equally to this paper.

Supporting information to DOI 10.1007/s12274-****-****-* (automatically inserted by the publisher)

1. Estimation of volumetric energy density

We estimated the volumetric energy density as follows.

According to SEM images, the density of ATO nanotubes is around 200 per 25 μm^2 (5 μm X 5 μm). The length of ATO nanotubes is 10 μm. Density of silicon is 2330 kg/m^3. The specific capacity of Si anode is 1500 mAh/g as measured. Based on these parameters, we estimate the volumetric energy density to be 2800 mAh/cm^3, which is 3.5 times of that of graphite (800 mAh/cm^3).

2. Analysis of first lithiation

In our experiment, TiO_2 nanotubes are fully covered by Si, which cut off the direct contact between TiO_2 and electrolyte. As the voltage went down to 1.5V from open-circuit voltage in the first lithiation, lithium ions in electrolyte cannot diffuse into TiO_2 without a direct contact as a feasible path. When the voltage reached 0.19 V, lithium ions can diffuse into Si, and can diffuse further into TiO_2. However, the total capacity of our TiO_2/Si composite is dominated by Si, and the contribution from TiO_2 is negligible as calculated below. Based on the TEM analysis in the main text, the TiO_2 nanotubes have inner radius of 150 nm and outer radius of 170 nm, while Si layer of 50 nm were coated on both inner and outer surface of TiO_2 nanotubes. The volume ratio of Si to TiO_2 is thus calculated to be 5:1. Taking Si density as 2330 kg/m^3 and TiO_2 density as 3840 kg/m^3, the mass ratio of Si to TiO_2 is calculated to be 2.75:1. The theoretical capacity of Si and TiO_2 are taken as 3590 mAh/g and 330 mAh/g, respectively. Thus, TiO_2 can only contribute about 3% of the total capacity of the composite.

Furthermore, after the first lithiation, TiO_2 nanotubes would remain lithiated during the first delithiation step and subsequent lithiation/delithiation cycles, as the voltage window is limited between 0.01 V and 1 V.

This analysis is also supported by cyclic voltammetry test at the scan rate of 0.1 mV/s (Fig. S1) and galvanostatic charge-discharge profile (Fig. S2) between OCV and 0.01V at the current rate of 140 mAh/g. Figure S1 shows no obvious peaks at 1.5 V- 1.7 V in the first lithiation, which confirms TiO_2 did not participate

in lithiation in this voltage window. In addition, Figure S2 shows no observable plateau at 1.5 V- 1.7 V. In conclusion, TiO_2 does not participated in lithiation before Si is lithiated at 0.2V as explained above.

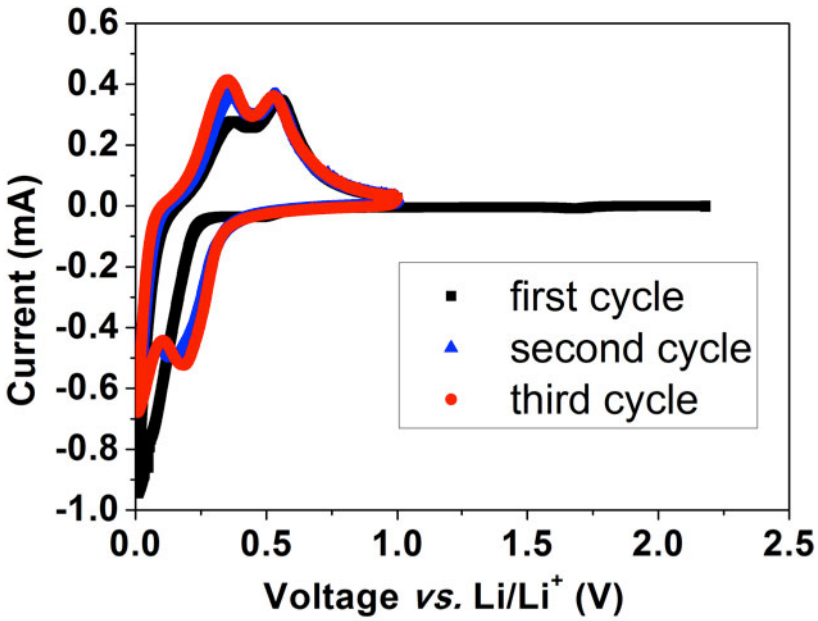

Figure S1. Cyclic voltammetry (CV) curves of coaxial Si-ATO-Si anode.

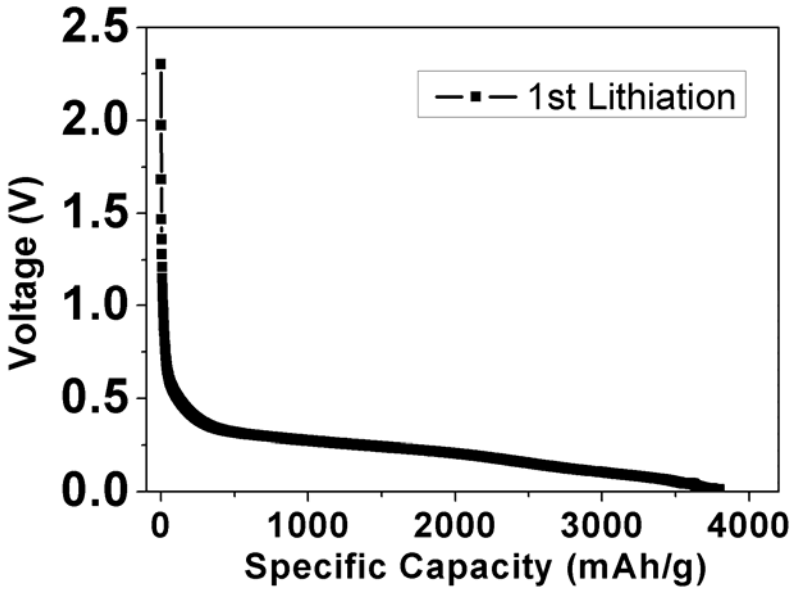

Figure S2. Galvanostatic charge-discharge voltage profile between OCV- 0.01V vs. Li/Li+ in the 1st cycle at 140 mA/g.

Table S1. Materials properties of Si used in simulation

Name	Symbol and unit	Value
Young's modulus	E (GPa)	47
Poisson's ratio	ν	0.278
Diffusion coefficient	D_0 ($m^2\ s^{-1}$)	1×10^{-16}
Density	($kg\ m^{-3}$)	2330
Partial molar volume	Ω ($m^3\ mol^{-1}$)	1.2×10^{-5}

Address correspondence to Chongwu Zhou, chongwuz@usc.edu